

A New Method for Simulating Embolic Coils as Heterogeneous Porous Media

HOOMAN YADOLLAHI-FARSANI ^{1,2} MARCUS HERRMANN,¹ DAVID FRAKES,^{2,3} and BRIAN CHONG^{2,4}

¹School for Engineering of Matter, Transport and Energy, Arizona State University, Tempe, AZ, USA; ²School of Biological and Health Systems Engineering, Arizona State University, 501 E Tyler Mall, BLDG ECG RM#334, Tempe, AZ 85287, USA; ³School of Electrical, Computer and Energy Engineering, Arizona State University, Tempe, AZ, USA; and ⁴Mayo Clinic Hospital, Phoenix, AZ, USA

(Received 21 June 2018; accepted 3 October 2018; published online 18 October 2018)

Associate Editors Dr. Ajit P. Yoganathan & Dr. Matthew J. Gounis oversaw the review of this article.

Abstract

Purpose—To gain insight into the influence of coils on aneurysmal hemodynamics, computational fluid dynamics (CFD) can be used. Conventional methods of modeling coils consider the explicit geometry of the deployed devices within the aneurysm and discretize the fluid domain. However, the complex geometry of a coil mass leads to cumbersome domain discretization along with a significant number of mesh elements. These problems have motivated a homogeneous porous medium coil model, whereby the explicit geometry of the coils is greatly simplified, and relevant homogeneous porous medium parameters are approximated. Unfortunately, since the coils are not distributed uniformly in the aneurysm, the homogeneity assumption is no longer valid.

Methods—In this paper, a novel heterogeneous porous medium approach is introduced. To verify the model, we performed CFD simulations to calculate the pressure drop caused by actual deployed coils in a straight cylinder. Next, we considered three different anatomical aneurysm geometries virtually treated with coils and studied the hemodynamics using the presented heterogeneous porous medium model.

Results—We show that the blood kinetic energy predicted by the heterogeneous model is in strong agreement with the conventional approach. The homogeneity assumption, on the other hand, significantly over-predicts the blood kinetic energy within the aneurysmal sac.

Conclusions—These results indicate that the benefits of the porous medium assumption can be retained if a heterogeneous approach is applied. Implementation of the presented method led to a substantial reduction in the total number of mesh elements compared to the conventional method, and

greater accuracy was enabled by considering heterogeneity compared to the homogenous approach.

Keywords—Brain aneurysm, CFD, Porous medium, Heterogeneous, Embolic coils.

INTRODUCTION

Endovascular coiling is frequently employed to treat unruptured brain aneurysms. One goal of the treatment is to reduce blood flow into the aneurysm and thereby promote thrombosis.¹⁴ Researchers have used computational fluid dynamics (CFD) to better understand the efficacy of coiling and the treatment's specific effects on aneurysmal hemodynamic.^{3,7,8} Unfortunately, the complexity of deployed embolic coils is such that considerable time and effort is required to generate high quality meshes of the devices. Additionally, small coil diameters demand a high number of boundary layer mesh elements, which results in high computational cost.² These issues have motivated researchers to look for less complex and costly ways of performing CFD on coiled aneurysms. Homogeneous porous medium theory is often applied to address the aforementioned modeling challenges.²⁹ Using this approach, endovascular coils are considered as homogeneous porous media to simplify the explicit geometries of the devices. In other words, local characteristics of the coil mass geometry do not influence local porosity and permeability—instead, both are held constant throughout the fluid domain of the coil mass.

Several works have implemented the homogeneity assumption. For example, in Refs. 18 and 23, authors considered coils as a homogeneous porous domain.

Address correspondence to Hooman Yadollahi-Farsani, School of Biological and Health Systems Engineering, Arizona State University, 501 E Tyler Mall, BLDG ECG RM#334, Tempe, AZ 85287, USA. Electronic mail: hyadolla@asu.edu

They observed that increasing the number of coils reduced the porosity, thereby decreasing intra-aneurysmal blood flow velocity. However, they mentioned that uneven distribution of coils within the aneurysmal sac invalidates the homogeneity assumption. A formula to calculate the minimum coil length needed to arrest blood flow in an aneurysm by applying the homogeneous porous medium assumption was derived in Ref. 19. In their paper, the homogeneous porous medium assumption was applied to overcome the difficulties associated with finding the permeability and porosity of a heterogeneous porous domain. Researchers in Ref. 24 attempted to assess the capability of the homogeneous porous medium assumption in comparison to the conventional approach of using explicit coil geometries. Specifically, they performed CFD simulations on explicit coil geometries and compared the results to those from simulations applying the homogeneous porous medium assumption. They concluded that despite the easier implementation of the homogeneous porous medium approach, it failed to capture the main flow features. Their results showed a significant deviation from the conventional approach.

In a recent work,²² the hemodynamics in physical models of two patient-specific aneurysms treated with coils were compared to those in a version of the same aneurysm embolized with a homogeneous porous medium. Authors showed that the homogeneity assumption considerably over-predicted blood flow into the aneurysm. Thus, despite the benefits associated with reduced computational cost and easier meshing, the non-uniform, complex geometries of coils degrade the homogeneity assumption. In other words, changes in porosity throughout the domain require a more sophisticated model that defines a position-dependent porosity map.

Experiments and numerical analyses performed in Ref. 27 quantified void spaces within the aneurysmal sac after coil deployment, and showed that the coil mass is not uniformly distributed. A Weibull distribution model was proposed to represent intra-aneurysmal pore distribution. The authors mentioned that the model could be used in numerical studies of intra-aneurysmal hemodynamics, but did not apply it themselves. As an alternative to numerical prediction of the permeability of a coil mass, experiments using a falling-head permeameter²⁸ and fluorescence microscopy¹⁰ can also be used.

In this paper, we present a novel method that considers coils as a heterogeneous porous medium. Specifically, the method applies the porous medium assumption but also considers non-uniform changes in domain porosity. First, we verified the capabilities of the proposed method in predicting pressure drop caused by coils placed in a straight cylinder. Next,

geometries of three different anatomical aneurysms were first constructed; embolic coils were then deployed virtually in each aneurysm using a finite element method (FEM). CFD simulations were performed on the explicit coil geometries, as well as corresponding homogeneous and heterogeneous porous domains.

MATERIALS AND METHODS

Governing Equations

The effect of a porous medium on the flow field was modeled by an added source term in the Navier–Stokes equation. The term was borrowed from the original Darcy’s law relating pressure drop to fluid velocity *via* permeability.^{11,12,17,31,32} Permeability and porosity were considered to be position-dependent 3D maps and were used as input for the Navier–Stokes equations.

$$\rho \left(\frac{\partial \mathbf{u}}{\partial t} + \nabla \cdot \left(\frac{\mathbf{u}\mathbf{u}}{\phi} \right) \right) = -\nabla p + \rho \mathbf{g} + \mu \nabla^2 \mathbf{u} - \frac{\mu \phi \mathbf{u}}{K} \quad (1)$$

In the equation above, ρ (kg/m³) is fluid density, \mathbf{u} (m/s) is superficial velocity, t (s) is time, ϕ is porosity, p (kg/m s²) is pressure, \mathbf{g} (m/s²) is gravity, μ (kg/ms) is dynamic viscosity, and K (m²) is permeability. Permeability was then calculated using the Carman–Kozeny relation.⁶ Defining porosity (ϕ) and specific area (A) per unit bulk volume as

$$\phi = \frac{\text{Device volume}}{\text{Total volume}} \quad (2)$$

$$A = \frac{\text{Internal surface area of the porous region}}{\text{Total volume}} \quad (3)$$

permeability is found

$$K = \frac{\phi^3}{cA^2} \quad (4)$$

where c is the shape factor. This factor is dependent on the cross section of the coils and was considered to be 2 in this study.⁶

Map Generation Procedure

Stereo-lithography (STL) representations of the deployed coil surfaces were used. This allowed us to take advantage of the triangular surface mesh to generate the porosity and permeability maps. The bounding box around each device was broken into a uniform lattice of hexahedra. Within each hexahedral, the device portion was closed by tessellating the open areas cut by the hexahedral faces. Once the device

portion within the hexahedral was watertight (Fig. 1), its area was found by adding the surface areas of all the triangles forming that device portion including the closure parts. The divergence theorem was then applied to calculate volume from surface area,¹ considering \vec{F} a vector field built from a triangle's corner and origin:

$$\Omega = \int_{\Omega} \nabla \cdot \vec{F}(x) d\Omega = \oint_S \vec{F} \cdot \hat{n} dS, \quad (5)$$

where Ω is the volume, S is the surface, and \hat{n} is the triangle's surface normal. The generated map was then used to find the porosity and permeability for each node in CFD mesh by means of tri-linear interpolation. This algorithm is explained further in “Appendix A”.

Numerical Method

The three-dimensional Navier–Stokes equations were solved using CLIFF (Cascade Technologies, Inc., Palo Alto, CA, USA). CLIFF is a second order node-based, incompressible solver and implements the fractional step method.^{15,16,20} The convergence criteria here was $1e-14$ for the pressure Poisson's solver. The walls were considered to be rigid and with a no-slip boundary condition. At the inlet, a constant inlet velocity was specified, and at the outlet, a convective outflow condition was used.

To ensure that the mean flow reached a steady state, kinetic energy per unit volume (Eq. 6) was calculated in the aneurysmal sac region and was tracked for five time units. The two-norm of the aneurysmal $K.E.$ was then calculated to ensure a sufficiently steady state solution. In other words, once the two-norm of the tracked data fell below a certain threshold (0.001), the flow was considered to be settled. These values are reported in “Appendix B”. In the following equation, $K.E.$ is kinetic energy per unit volume (kg/ms^2), \forall (m^3) is total volume of cells, \forall_i (m^3) is individual mesh cell's

volume, ρ (kg/m^3) is fluid density, and $\mathbf{u}_{\text{physical}}$ (m/s) is mesh cell's physical velocity:

$$K.E. = \frac{\rho}{2} \left(\frac{1}{\forall} \sum_i \forall_i \|\mathbf{u}_{\text{physical}}\|_i^2 \right). \quad (6)$$

The physical velocity is a more realistic and accurate representation of velocity in porous region and is specified as³³:

$$\mathbf{u}_{\text{physical}} = \frac{\mathbf{u}}{\phi}. \quad (7)$$

Verification Model

To verify the porous medium approach suggested here, the common methodology which was first suggested by Darcy in 1856^{5,30} was used here. In this approach, the pressure drop across a porous medium is related to the volumetric flow rate in a steady flow. To replicate this process, a straight cylinder with a sphere in the middle was made and then 3D printed (Fig. 2). The model helped with isolating the effects of the porous region on the domain from any other variabilities caused by an actual patient-specific aneurysmal geometry. One TruFill DCS Orbit coil (Codman Neurovascular, Johnson & Johnson, Brunswick, NJ) with length and deployed outer diameter of 0.15 m and 0.009 m, respectively, was considered to be the porous medium investigated here and was deployed in the spherical part of the model. Once the coils were deployed, μCT images were acquired using a Siemens Inveon μCT scanner. The in-plane and out of plane resolutions were $28.4 \mu\text{m}$ with a total number of $1024 * 1024$ pixels on each slice. Given the individual coil diameter of $304.8 \mu\text{m}$, there existed almost 11 pixels in each coils' cross section. Images were then imported into Mimics software (Materialize, Ann Arbor, MI) to reconstruct the coils' geometries. Segmentation of images was done using thresholding and region growing (Fig. 2). It should be noted that no scanner can capture gaps between adjacent coil wires that are considerably smaller than the scanner's resolution. Some of the artifacts apparent in the geometry shown in Fig. 2, including the appearance of coil wire diameter variations and merging, are the result of resolution limitations. Nevertheless, the same baseline geometries were used in this study as inputs to the conventional CFD approach, the homogeneous porous medium approach, and the proposed heterogeneous porous medium approach. To ensure that the presented porous medium model was examined at different flow scenarios including viscous or inertia dominant, three different Reynolds numbers were considered. We first considered a Reynolds number of

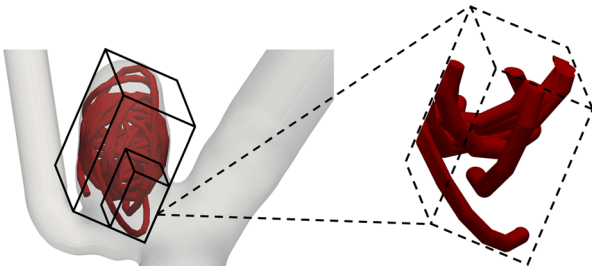


FIGURE 1. Watertight sub-domain (right) of the porous region (left). Device portion within the smaller hexahedral has been determined and magnified as an example.

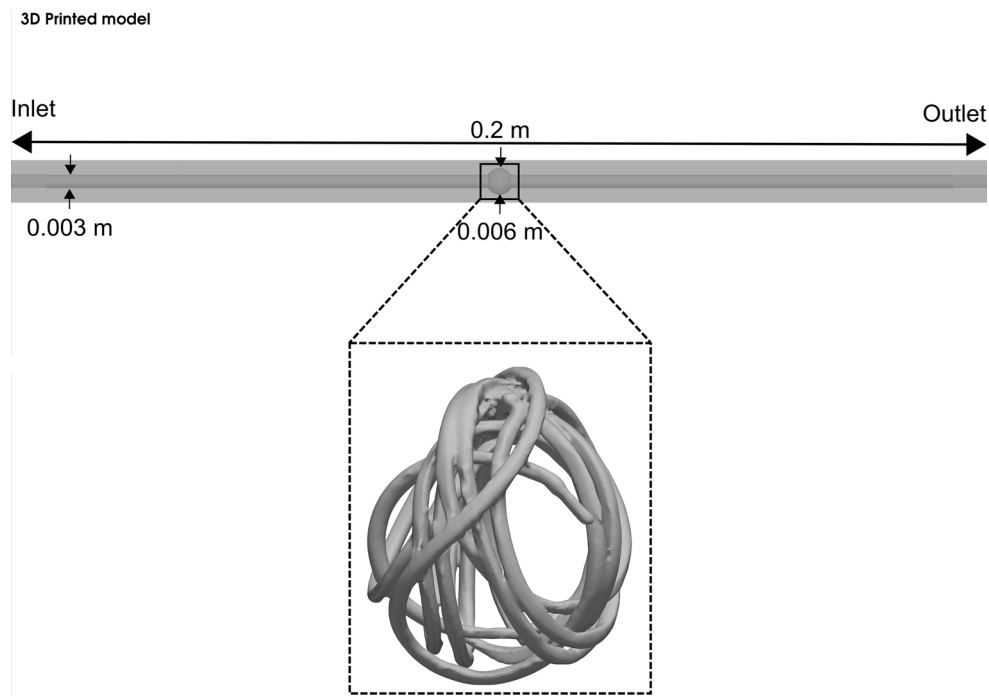


FIGURE 2. Verification model (top) and the reconstructed porous medium (coils).

4.7 which was associated with the inflow at the aneurysmal neck in one of the anatomical geometries (case A). For a viscous dominant flow a Reynolds number of 0.5, and for an inertia dominant flow, a Reynolds number of 10 were then considered. It is mentioned that these Reynolds numbers are based on an individual coil diameter.

Anatomical Models

The simulations for anatomical geometries (Fig. 3) were run at a constant input volumetric flow rate of 2 mL/s.¹³ Blood in the anatomical geometries was considered to be incompressible, Newtonian, and with a density and viscosity of 1060 (kg/m³) and 0.00371 (kg/ms),²¹ respectively. Based on the parent vessel inlet diameters of 0.0028 m (model A), 0.0027 m (model B), 0.0029 m (model C), the Reynolds numbers were 253, 266, and 251, respectively. Additionally, the Reynolds numbers (based on the individual coil diameter) at the aneurysmal neck for cases A, B, and C were 4.7, 7.2, and 25.7, respectively.

To create the three anatomical cerebral aneurysms, computed tomography (CT) images were acquired. The images had matrix sizes of 512 * 512 and a slice thickness of 625 μ m. The raw images were anonymized prior to research use, enhanced with custom software written in MATLAB (MathWorks, Natick, MA, USA), and then imported into Mimics software (Ma-

terialise, Leuven, Belgium). Reconstructed models were then modified to ensure that the inlet length was sufficient for flow to fully develop⁹ (Fig. 3). The total inlet lengths for models A, B and C were 0.0681, 0.0679, and 0.0680 m, respectively. Endovantage Suite (Endovantage, LLC, Scottsdale, AZ, USA) was used to deploy coils into the aneurysm geometries. This suite replicates the actual deployment procedure and takes into account the mechanical properties of the coils.^{3,4} All geometries were then imported into ANSYS ICEM 16.2 (ANSYS, Inc., Canonsburg, PA, USA) and an initial mesh was generated. Due to the complexity of the anatomical aneurysm geometries and the coils, tetrahedral mesh elements were used to discretize the fluid domain. To capture the sharp velocity gradients at the walls, refined mesh regions near the walls were utilized (Fig. 4). The initial mesh was then refined twice using ANSYS FLUENT 16.2 (ANSYS, Inc., Canonsburg, PA, USA); this was done by refining all the edges by a factor of 2. This led to 3 different meshes: a coarse, medium and fine mesh.

Grid-Independence Study

The independence of the solution from the generated mesh was then examined by the method presented by Roache.²⁶ This approach, based on the so-called Grid Convergence Index (GCI), is used to estimate errors due to domain discretization. In other words,

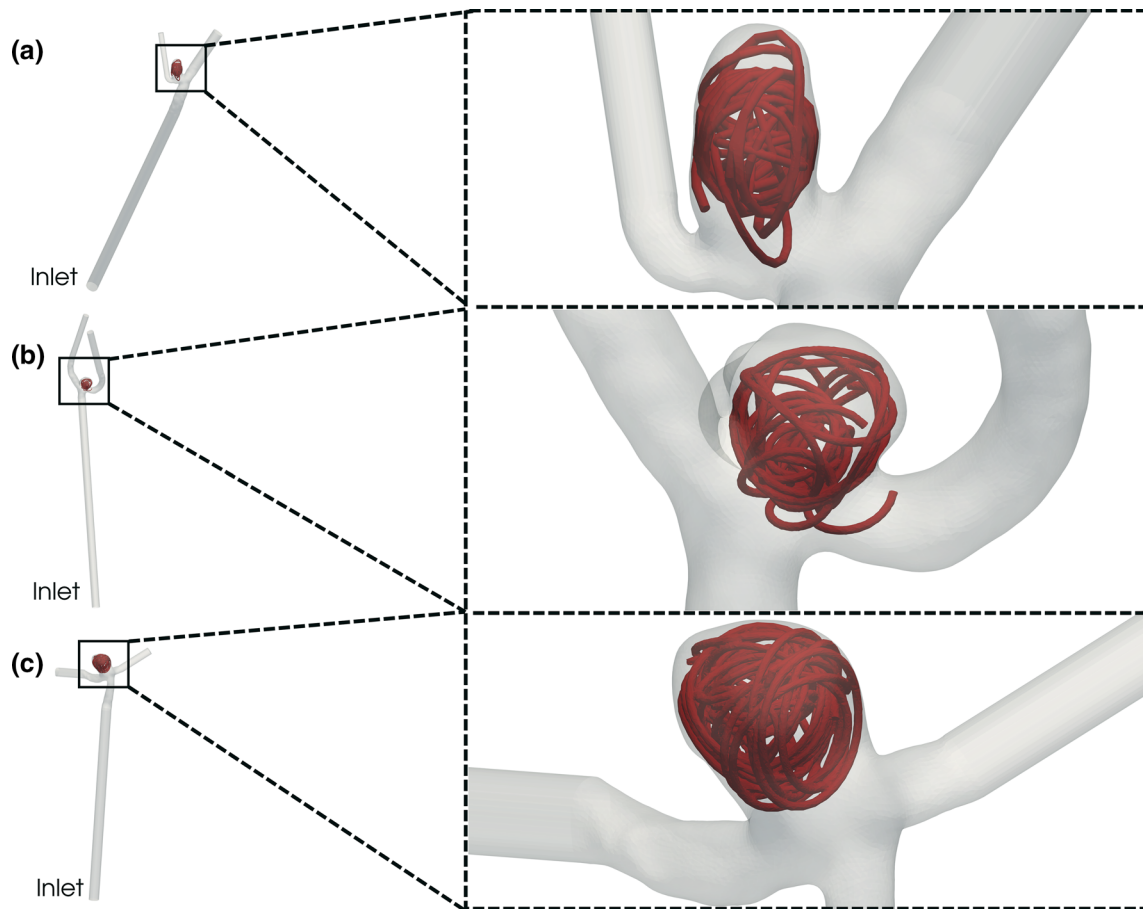


FIGURE 3. Treated aneurysm with FEM coils, (a) first case (b) second case (c) third case. The entire anatomical models are shown on left and the saccular regions on right. Inlets for each model are indicated on the figure for clarity, the remaining branches were considered as outlets.

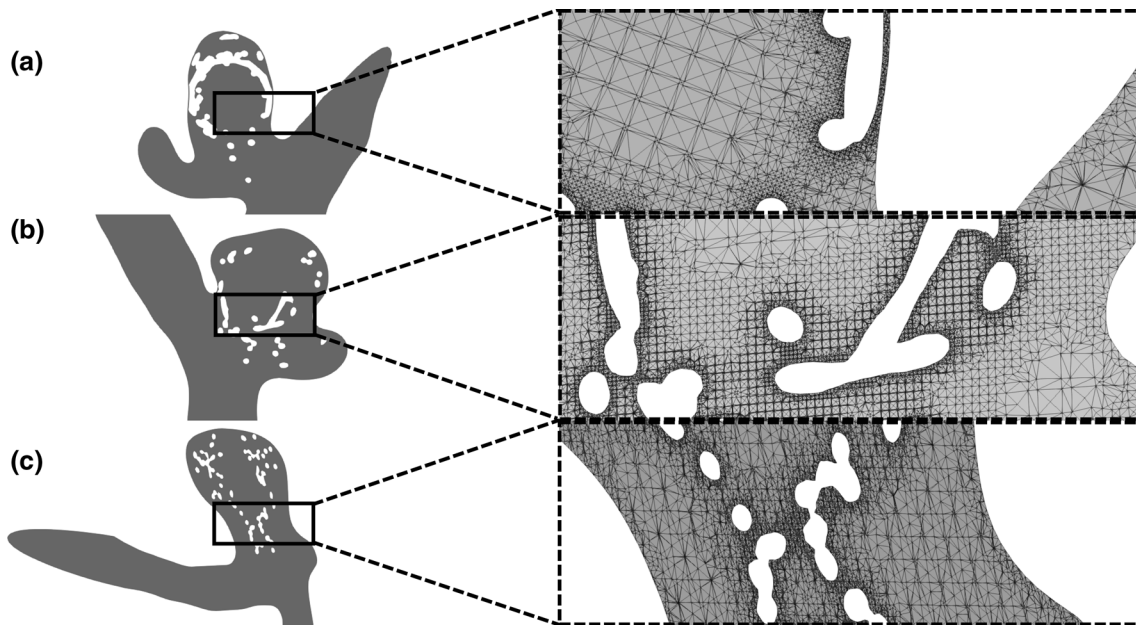


FIGURE 4. Near wall refinements for the anatomical models, (a) first case (b) second case (c) third case.

GCI measures the deviation of a computed value from the asymptotic value at infinite mesh resolution. The asymptotic value is predicted by utilizing Richardson extrapolation based on the values from the two finest grids. The details for the mesh refinement study are given in “Appendix B”. As it is seen, the error bands for all the cases are quite small ($1.2795E-0.3-0.26\%$); this confirms that our solution is not affected by discretization errors.

RESULTS

Verification Model

Pressure drops across the entire model were calculated based on CFD simulations. These included the model devoid of the coils (untreated), explicitly coiled (treated) model, homogeneous porous medium model, and the presented heterogeneous porous medium model at different map resolutions. Note that resolution here refers to the number of hexahedra in each axial direction that were used in the mapping algorithm. To apply the heterogeneity assumption, porosity maps at different resolutions were generated and visualized on a cut passing through the middle of the model (Fig. 5). It is evident from the figure that refinement of the porosity map resolution resulted in the better description of the coils’ configurations.

The calculated pressure drops are shown in Fig. 6. To isolate the pressure drop caused by the porous structure (coils), the pressure drop associated with the model devoid of coils (untreated) was subtracted from the numbers reported in this figure. With porosity map refinement, the pressure drops predicted by the heterogeneous porous medium model approaches the value obtained from the CFD simulations when the explicit geometry of coil mass was available (treated). The pressure drops predicted by resolutions 32, and 64 show a good agreement with the treated model. For

example, at the Reynolds number of 4.7, these deviations are 0.5 and 3% for map resolutions of 32 and 64, respectively. Additionally, the homogeneous porous medium assumption under-predicts the pressure drop considerably.

To better understand the capability of the heterogeneity assumption in capturing the main flow features, snapshots of velocity magnitude contours were generated on a cut plane passing through the center of the model. In Fig. 7, the snapshots of velocity in the domain for different Reynolds numbers are shown. The left, middle, and right columns correspond to the Reynolds numbers of 0.5, 4.7, and 10, respectively. As shown, the homogeneous medium (HG) fails to predict a flow field which is similar to the one from the explicitly coiled geometry. However, the heterogeneous map shows overall flow structures that are very similar to the explicitly coiled geometry.

Anatomical Models

Cuts through the treated aneurysms containing explicit coil geometries, as well as three porosity map resolutions are given in Fig. 8. As is shown, the more refined the porosity map, the better the description of the coil’s geometry. To quantify the effect of porosity map resolution on aneurysmal hemodynamics, the kinetic energy per unit volume ($K.E.$) for each case was calculated in the saccular region. In Fig. 9, $K.E.$ magnitudes for each case are shown. Reported values in this figure include the untreated and explicitly coiled geometries (treated) as well as the porous medium assumptions. As the results given in Fig. 9 show, deploying the coils led to aneurysmal $K.E.$ reductions of 80.77, 84.30 and 67.67% with respect to the untreated geometry for cases A, B, and C, respectively. Furthermore, the homogeneity assumption overestimated $K.E.$ by 268.42, 414.67 and 98.07% for cases A, B, and C, respectively. The refinement of the heterogeneous porous domain allowed the $K.E.$ values to

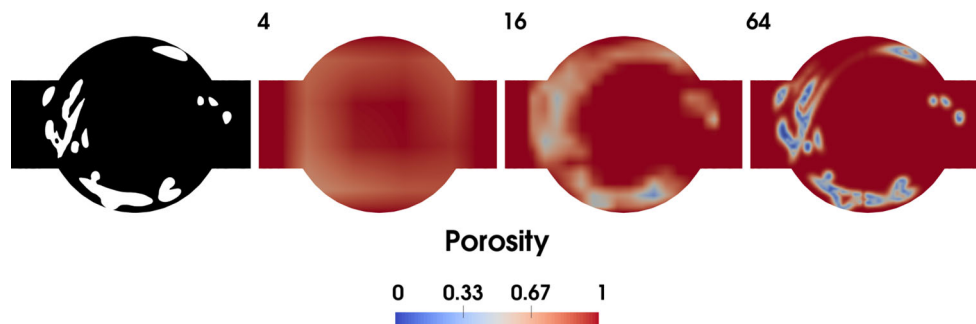


FIGURE 5. Porosity maps at different resolutions for the verification model. Numbers on each subfigure show the number of hexahedra in each axial direction.

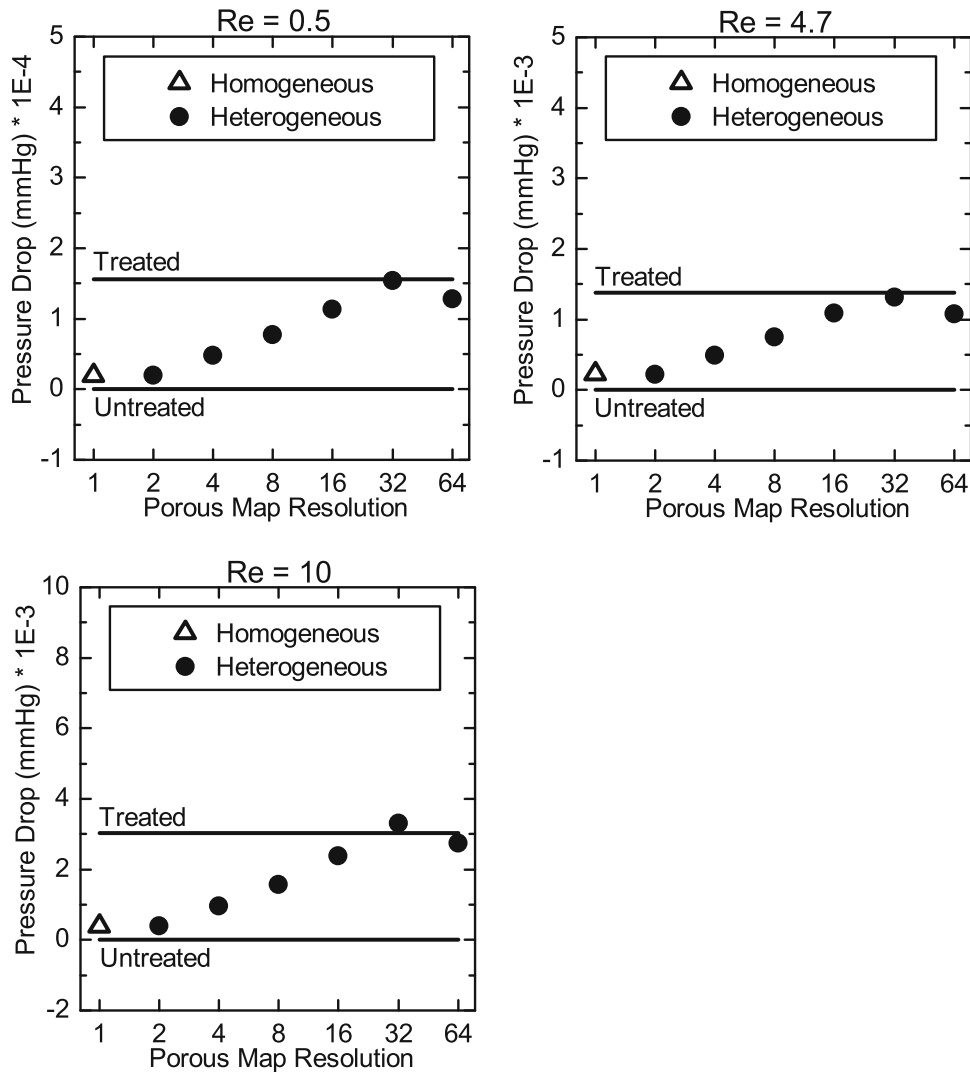


FIGURE 6. Porous medium pressure drop values in the verification model and for all Reynolds numbers. The solid lines show the values for the explicitly coiled geometries (treated) and the untreated models.

approach those from the explicitly coiled (treated) aneurysm. For example, the absolute errors at the map with 64 hexahedra in each axial direction for cases A, B, and C were 9.25, 1.87 and 1.92%, respectively.

To better visualize the effect of porous medium assumption on aneurysmal hemodynamics, snapshots of velocity streamlines are shown in Fig. 10. The first column represents the velocity streamlines in the aneurysm in the presence of the explicit coil geometries. As the figure shows, the flow path predicted by the homogeneous porous domain (HG) is not similar to the explicitly coiled geometry. To demonstrate the capability of the heterogeneity assumption, streamlines associated with the porosity map resolution of 64 were generated. It is apparent from Fig. 10 that flow path

captured by the heterogeneous porous map are in better agreement with one from the explicitly coiled geometry.

DISCUSSION

Reducing aneurysmal blood flow velocity promotes thrombosis in the aneurysmal sac and may prevent rupture and hemorrhage. The results reported in Ref. 25 also show that aneurysmal flows in untreated geometry are far more active than in the treated counterpart. Nonetheless, as other studies have shown, the rather complex geometries of coils make the CFD simulations extremely complicated and computationally very expensive.² The detailed results tabulated in

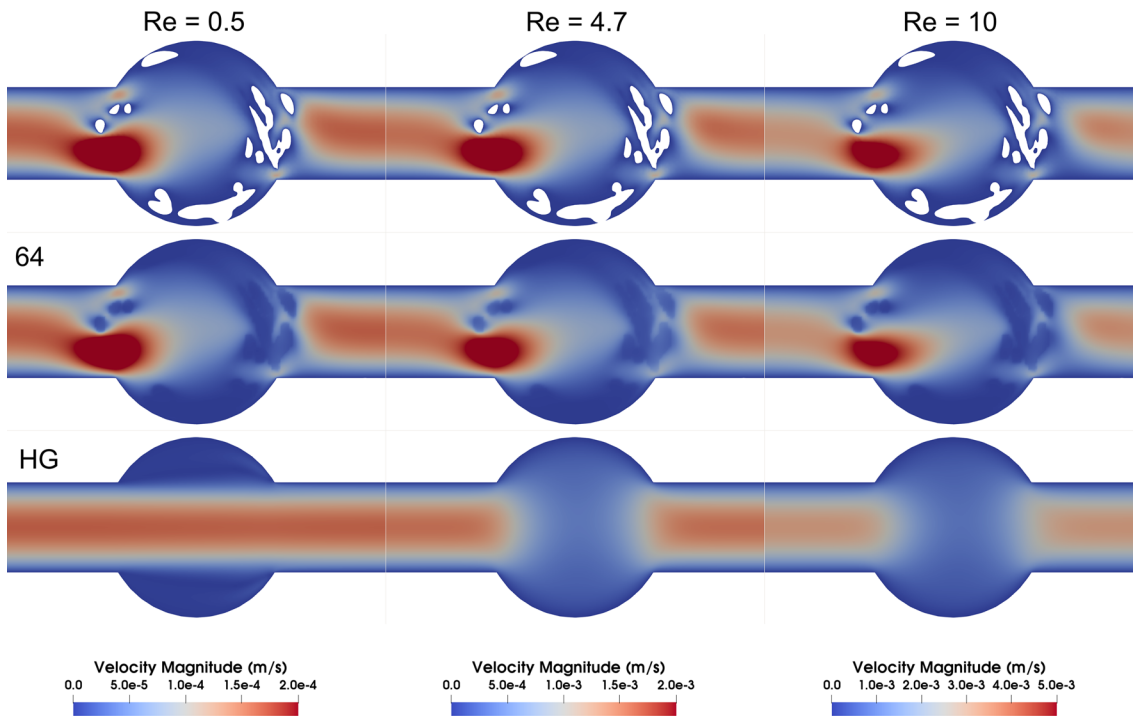


FIGURE 7. Snapshots of velocity contours in the verification model and for all Reynolds numbers. HG corresponds to the homogeneous porous medium assumption, and 64 pertains to the map resolution 64.

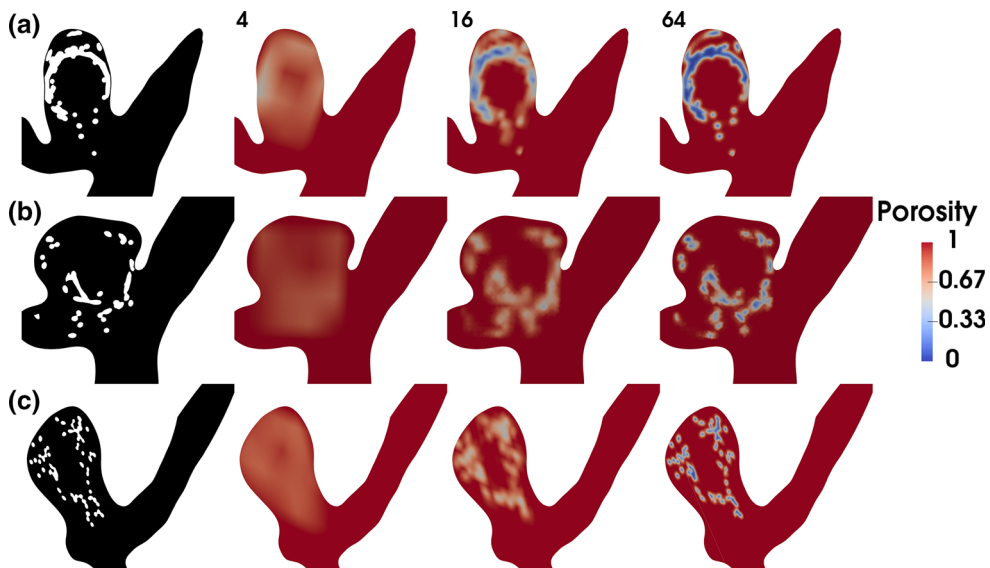


FIGURE 8. Porosity maps at different resolutions for the anatomical cases A, B and C. Numbers on each subfigure show the number of hexahedra in each axial direction. The first column represents the anatomical models in presence of the explicit geometry of coils.

“Appendix B” also reveal the same fact. Specifically, the total mesh elements needed to discretize treated geometries are, on average, twice as many as those needed for the untreated geometries.

Unfortunately, the conventional solution to these problems, which is using the homogeneous porous domain, has not been able to produce meaningful results. Previous studies have reported the inability of this

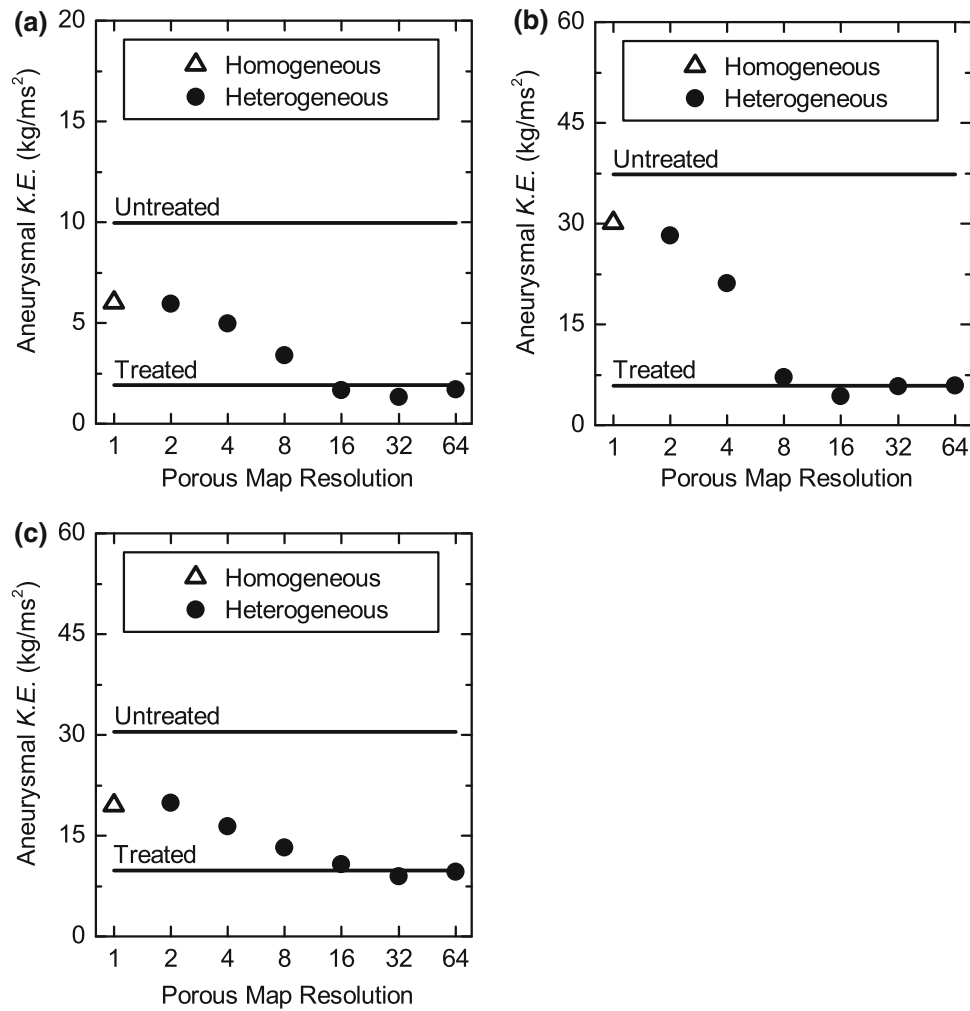


FIGURE 9. Aneurysmal kinetic energy (K.E.) values for the anatomical cases A, B, and C. The solid lines show the values for the explicitly coiled geometries (treated) and the untreated models.

method to correctly predict flow stagnation in the aneurysm.²² Aneurysmal *K.E.* (Fig. 9), a representative of intra-aneurysmal hemodynamics, reported an over-prediction that is in accordance with the results reported in Ref. 22. This is due to the fact that coil masses are complex geometries with large variations in porosity and permeability. Since coils are inclined to rest against the aneurysmal wall, the coil mass is much denser in near-wall regions as well as at the neck of the aneurysm. As the flow of blood into the sac passes through the neck region, it is important to accurately estimate flow resistance in this area. The homogeneity assumption distributes the porosity and permeability in a way that porosity at the

neck of the aneurysm is over-predicted and thus, there is less resistance to blood flow than in reality.

We suggested a novel way of simulating coils as a heterogeneous porous domain that, to the best of our knowledge, has not been proposed before. As our results show, implementation of the heterogeneity assumption provided a more accurate representation of coils. We showed that a porous domain with 16 hexahedra in each direction is refined enough to accurately predict the coils' effects on *K.E.* in aneurysmal sac. The non-uniform spatial distribution of porosity led to a more realistic porous domain. The accurate representation of the coils, especially at the

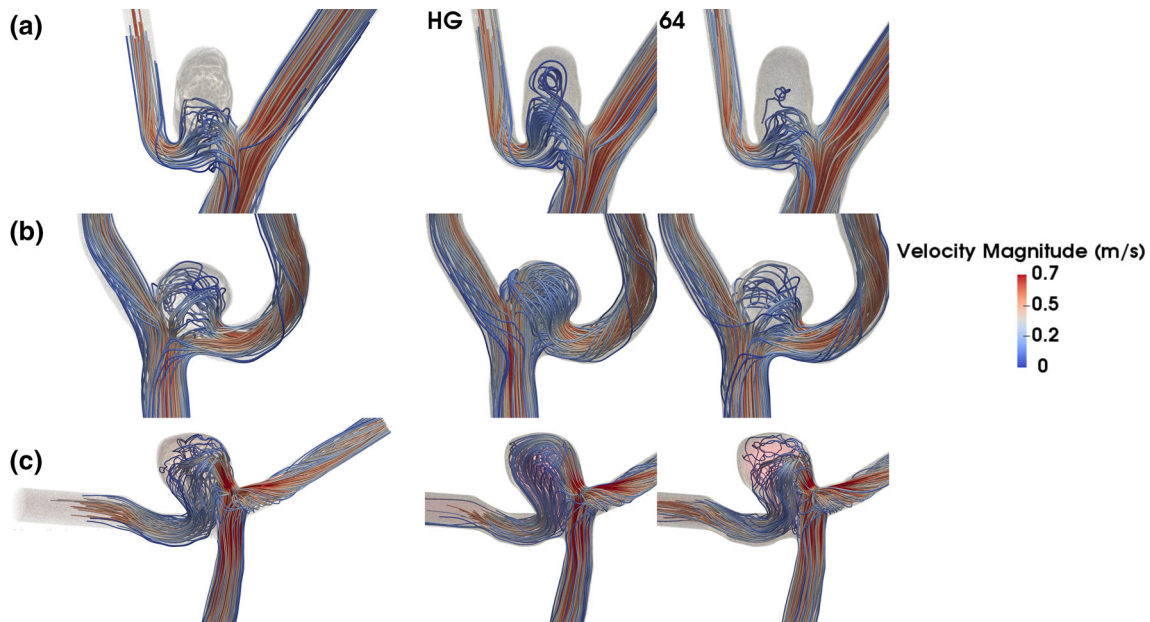


FIGURE 10. Velocity streamlines for the anatomical cases A, B and C. From left to right: the coiled geometry, homogeneous porous medium (HG) and heterogeneous map with 64 hexahedra in each axial direction.

neck of the aneurysm, provided a resistance distribution that is comparable to that from the explicitly coiled geometry. Our verification data show that the pressure drop predicted by the heterogeneous model agrees well with the data obtained from the explicitly coiled model. In contrast, the pressure drops predicted by the homogeneous porous medium approach are significantly under-predicted.

Use of the proposed method helped us significantly reduce computational expense by removing boundary layer mesh elements on the coils. It is also noteworthy that the mesh we used for porous medium simulations was the same one used for the untreated geometry. In other words, having a single untreated meshed geometry enabled us not only to study the untreated aneurysm, but also to study the treated geometry when the heterogeneous porous medium assumption is applied. Additionally, implementation of the heterogeneous porous domain assumption eliminates the need to perform CFD simulations on explicitly coiled geometries. Moreover, as the data in the “Appendix” suggest for untreated geometries, a relatively coarse mesh (MESH#2) can be used as all three meshes are in the asymptotic regime of mesh convergence ($ARC \equiv$

1). It is also worth mentioning that the implementation of the proposed method enables one to study multiple coil deployments in an aneurysm without the need for remeshing. Lastly, the proposed method can be used to quantify intra-aneurysmal void spaces as well, toward use of a statistical model to represent the coils.²⁷

In order to quantify the computational resources saved, the number of core-hours consumed by each simulation was recorded. By eliminating the need to perform CFD simulations for the explicitly coiled geometries and considering that the middle level mesh (MESH#2) for the untreated geometry was refined sufficiently (as the reported values are well within the asymptotic range of convergence), we were able to speed up the total simulation run time by a factor greater than 5 (case A). For example, the total number of core-hours needed to perform CFD simulations on all three meshes for the explicitly coiled geometries in case A was almost 30,000. Core-hours used for the untreated geometry (MESH#2) was about 6000 in case A. These numbers for cases B and C were roughly 35,000 and 43,000 for the explicitly coiled geometries (all three meshes) and 5000 and 6000 for the untreated

geometries (MESH#2), respectively. This provides speed up factors of 7 and 7.2 for cases B and C, respectively.

CONCLUSIONS

This study showed that when coils are modeled using the homogeneity assumption, considerable errors in predicting intra-aneurysmal $K.E.$ can occur. This is mainly due to the fact that the Carman–Kozeny equation is dependent on the geometry of the porous medium and the homogeneity assumption does not take into consideration the non-uniform changes in the porous domain. In other words, the heterogeneity assumption which considers the non-uniform changes can provide a deterministic way of calculating permeability using the Carman–Kozeny relation. The reported data in this study showed that a refined enough heterogeneous porous domain that represents the explicit geometry, can predict intra-aneurysmal $K.E.$ and the main flow features, while reducing computational cost.

APPENDIX A

Algorithm used to generate the porosity and permeability maps:

- (1) Read in the STL file.
- (2) Break the domain into a lattice of hexahedra.
- (3) For each hexahedral, find the colliding surface mesh triangles.
- (4) Watertight the coil portion which falls within the hexahedral by closing the open faces.
- (5) Find the porosity (coil volume/sac volume).
- (6) Use the Carman-Kozeny equation to find permeability.
- (7) Associate each porosity/permeability to its position in the CFD mesh using a tri-linear interpolation method and generate the map.
- (8) Use the generated map as an input for the source term in momentum equation.

APPENDIX B

See Tables [1](#), [2](#), [3](#), [4](#), [5](#), and [6](#).

TABLE 1. Total number of mesh elements for the cases considered in the study.

	Case A		Case B		Case C		Verification model	
	Untreated	Treated	Untreated	Treated	Untreated	Treated	No coils	With coils
MESH 1	2,161,693	4,845,441	2122092	5,953,263	2,499,877	4,935,209	3,131,916	6,681,183
MESH 2	17,293,544	38,763,528	16,976,736	47,626,104	19,999,016	39,481,672	25,412,764	53,449,464
MESH 3	138,348,352	310,108,224	135,813,888	381,008,832	159,992,128	315,853,376	205,446,728	427,595,712

TABLE 2. Aneurysmal K.E. (kg/ms²) for the anatomical cases considered in the study.

	Case A		Case B		Case C	
	Untreated	Treated	Untreated	Treated	Untreated	Treated
MESH 1	9.8445	1.9034	36.8488	5.8665	30.5252	9.8177
MESH 2	9.9898	1.9167	37.3665	5.8669	30.7060	9.8761
MESH 3	9.9744	1.9167	37.3502	5.8672	30.6102	9.8675

TABLE 3. Pressure drop values (mmHg) found numerically across the verification model.

	Treated
MESH 1	0.5794
MESH 2	0.5700
MESH 3	0.5689

TABLE 5. Grid Convergence Index (GCI) analysis for the coiled verification model based on pressure drop values.

	Verification model
P	3.1204
GC23 (%)	0.03
GC12 (%)	0.26
fh0	0.5687
ARC	1.0164

TABLE 4. Grid Convergence Index (GCI) analysis for the anatomical models based on aneurysmal K.E. (kg/ms²).

	Case A		Case B		Case C	
	Untreated	Treated	Untreated	Treated	Untreated	Treated
P	3.2360	8.0274	4.9873	0.9999	0.9160	2.7737
GC23 (%)	0.02	1.2795E-05	1.7774E-03	4.7525E-03	0.43	0.01
GC12 (%)	0.21	3.3618E-03	0.05	9.5056E-03	0.83	0.12
fh0	9.9726	1.9167	37.3497	5.8674	30.5021	9.8661
ARC	0.9854	0.9930	0.9861	0.9999	0.9941	0.9940

TABLE 6. Two-norms calculated for different cases in the numerical studies for Mesh 2.

	Case A		Case B		Case C		Verification model	
	Untreated	Treated	Untreated	Treated	Untreated	Treated	No coils	With coils
	3.0447E-05	2.7839E-06	6.5315E-05	8.4261E-06	1.1874E-05	3.7868E-05	1.0286E-04	2.5889E-04

ACKNOWLEDGMENTS

We would like to acknowledge the support from the National Science Foundation (Award #1512553). We would like to thank Endovantage, LLC for providing us with the numerical coil deployments.

FUNDING

This study was funded by NSF (Award #1512553).

CONFLICT OF INTEREST

Author Hooman Yadollahi-Farsani, Author Marcus Herrmann, Author David Frakes, and Author Brian Chong declare that they have no conflicts of interest.

ETHICAL APPROVAL

This article does not contain any studies with human participants or animals performed by any of the authors.

REFERENCES

- ¹Arvo, J. Graphics Gems II. San Diego: Academic Press, 1991.
- ²Augsburger, L., P. Reymond, D. A. Rufenacht, and N. Stergiopoulos. Intracranial stents being modeled as a porous medium: flow simulation in stented cerebral aneurysms. *Ann. Biomed. Eng.* 39:850–863, 2011.
- ³Babiker, M. H., B. Chong, L. F. Gonzalez, S. Cheema, and D. H. Frakes. Finite element modeling of embolic coil deployment: multifactor characterization of treatment effects on cerebral aneurysm hemodynamics. *J. Biomech.* 46:2809–2816, 2013.
- ⁴Babiker, M. H., L. F. Gonzalez, J. Ryan, F. Albuquerque, D. Collins, A. Elvikis, and D. H. Frakes. Influence of stent configuration on cerebral aneurysm fluid dynamics. *J. Biomech.* 45:440–447, 2012.
- ⁵Bear, J. Dynamics of Fluids in Porous Media. New York: Dover, 1972.
- ⁶Carman, P. C. Flow of Gases Through Porous Media. New York: Academic Press, 1956.
- ⁷Cha, K. S., E. Balaras, B. B. Lieber, C. Sadasivan, and A. K. Wakhloo. Modeling the Interaction of coils with the local blood flow after coil embolization of intracranial aneurysms. *J. Biomech. Eng.* 129:873–879, 2007.
- ⁸Chalouhi, N., S. Tjoumakaris, R. M. Starke, L. F. Gonzalez, C. Randazzo, D. Hasan, J. F. McMahon, S. Singhal, L. A. Moukarzel, A. S. Dumont, R. Rosenwasser, and P. Jabbour. Comparison of flow diversion and coiling in large unruptured intracranial saccular aneurysms. *Stroke* 44:2150–2154, 2013.
- ⁹Chaudhury, R. A., M. Herrmann, D. H. Frakes, and R. J. Adrian. Length and time for development of laminar flow in tubes following a step increase of volume flux. *Exp. Fluids* 56:22, 2015.
- ¹⁰Chueh, J.-Y., S. Vedantham, A. K. Wakhloo, S. L. Carniato, A. S. Puri, C. Bzura, S. Coffin, A. A. Bogdanov, and M. J. Gounis. Aneurysm permeability following coil embolization: packing density and coil distribution. *J. NeuroInterventional Surg.* 2014. <https://doi.org/10.1136/neurintsurg-2014-011289>.
- ¹¹Ergun, S. Fluid flow through packed columns. *Chem. Eng. Prog.* 48:89–94, 1952.
- ¹²Ergun, S., and A. A. Orning. Fluid flow through randomly packed columns and fluidized beds. *Ind. Eng. Chem.* 41:1179–1184, 1949.
- ¹³Gascou, G., R. Ferrara, D. Ambard, M. Sanchez, K. Lobotesis, F. Jourdan, and V. Costalat. The pressure reduction coefficient: a new parameter to assess aneurysmal blood stasis induced by flow diverters/disruptors. *Interv. Neuroradiol.* 23:41–46, 2017.
- ¹⁴Guglielmi, G., F. Viñuela, J. Dion, and G. Duckwiler. Electrothrombosis of saccular aneurysms via endovascular approach. *J. Neurosurg.* 75:8–14, 1991.
- ¹⁵Ham, F., and G. Iaccarino. Energy Conservation in Collocated Discretization Schemes on Unstructured Meshes. Annual Research Briefs. Stanford: Center for Turbulence Research, Stanford University, pp. 3–14, 2004.
- ¹⁶Ham, F., and K. Mattsson. Accurate and stable finite volume operators for unstructured flow solvers. Annual Research Briefs. Stanford: Center for Turbulence Research, Stanford University, pp. 243–261, 2006.
- ¹⁷Hsu, C. T., and P. Cheng. Thermal dispersion in a porous medium. *Int. J. Heat Mass Transf.* 33:1587–1597, 1990.
- ¹⁸Kakalis, N. M. P., A. P. Mitsos, J. V. Byrne, and Y. Ventikos. The haemodynamics of endovascular aneurysm treatment: a computational modelling approach for estimating the influence of multiple coil deployment. *IEEE Trans. Med. Imaging* 27:814–824, 2008.
- ¹⁹Khanafar, K., R. Berguer, M. Schlicht, and J. L. Bull. Numerical modeling of coil compaction in the treatment of cerebral aneurysms using porous media theory. *J. Porous Media* 12:887–897, 2009.
- ²⁰Kim, J., and P. Moin. Application of a fractional-step method to incompressible Navier-Stokes equations. *J. Comput. Phys.* 59:308–323, 1985.
- ²¹Kundu, P. K., I. M. Cohen, and D. R. Dowling. Fluid Mechanics. New York: Academic Press, 2012.
- ²²Levitt, M. R., M. C. Barbour, S. Rolland du Roscoat, C. Geindreau, V. K. Chivukula, P. M. McGah, J. D. Nerva, R. P. Morton, L. J. Kim, and A. Aliseda. Computational fluid dynamics of cerebral aneurysm coiling using high-resolution and high-energy synchrotron X-ray microtomography: comparison with the homogeneous porous medium approach. *J. NeuroInterventional Surg.* 2016. <https://doi.org/10.1136/neurintsurg-2016-012479>.
- ²³Mitsos, A. P., N. M. P. Kakalis, Y. P. Ventikos, and J. V. Byrne. Haemodynamic simulation of aneurysm coiling in an anatomically accurate computational fluid dynamics model: technical note. *Neuroradiology* 50:341–347, 2008.
- ²⁴Morales, H. G., I. Larrabide, M. L. Aguilar, A. J. Geers, J. M. Macho, L. S. Roman, and A. F. Frangi. Comparison of two techniques of endovascular coil modeling in cerebral aneurysms using CFD. In: 2012 9th IEEE International Symposium on Biomedical Imaging (ISBI), 2012. <https://doi.org/10.1109/isbi.2012.6235780>.

- ²⁵Nair, P., B. W. Chong, A. Indahlastari, J. Ryan, C. Workman, M. Haithem-Babiker, H. Yadollahi Farsani, C. E. Baccin, and D. Frakes. Hemodynamic characterization of geometric cerebral aneurysm templates treated with embolic coils. *J. Biomech. Eng.* 138:021011, 2016.
- ²⁶Roache, P. J. Perspective: a method for uniform reporting of grid refinement studies. *J. Fluids Eng.* 116:405–413, 1994.
- ²⁷Sadasivan, C., J. Brownstein, B. Patel, R. Dholakia, J. Santore, F. Al-Mufti, E. Puig, A. Rakian, K. D. Fernandez-Prada, M. S. Elhammady, H. Farhat, D. J. Fiorella, H. H. Woo, M. A. Aziz-Sultan, and B. B. Lieber. In vitro quantification of the size distribution of intrasaccular voids left after endovascular coiling of cerebral aneurysms. *Cardiovasc. Eng. Technol.* 4:63–74, 2013.
- ²⁸Sadasivan, C., E. Swartwout, A. D. Kappel, H. H. Woo, D. J. Fiorella, and B. B. Lieber. In vitro measurement of the permeability of endovascular coils deployed in cerebral aneurysms. *J. NeuroInterventional Surg.* 2018. <https://doi.org/10.1136/neurintsurg-2017-013481>.
- ²⁹Vafai, K. *Porous Media: Applications in Biological Systems and Biotechnology*. Boca Raton: CRC Press, 2010.
- ³⁰Vafai, K. *Handbook of Porous Media* (3rd ed.). Boca Raton: CRC Press, 2015.
- ³¹Wang, L., L.-P. Wang, Z. Guo, and J. Mi. Volume-averaged macroscopic equation for fluid flow in moving porous media. *Int. J. Heat Mass Transf.* 82:357–368, 2015.
- ³²Whitaker, S. Flow in porous media I: A theoretical derivation of Darcy's law. *Transp. Porous Media* 1:3–25, 1986.
- ³³Whitaker, S. *The Method of Averaging*. New York: Springer, 1998.